Bulletin of the Geological Society of Malaysia, Volume 76, November 2023, pp. 27 - 45
DOI: https://doi.org/10.7186/bgsm76202303

Ion adsorption-type rare earth element deposits in western Peninsular Malaysia: A case study in Bukit Enggang Granite, Kedah

Fakhruddin Afif Fauzi[1,*], Edwin James[2], Muhammad Sufi Musa[3], Hamdan Ariffin[1], Abdullah Sulaiman[4], Mahat Sibon[5], Abdul Hadi Abdul Rahman[6], Muhammad Falah Zahri[3], Azizan Ali[1]

[1]Department of Mineral and Geoscience Kedah/Perlis/P. Pinang, Jln. Perak, Off Jalan Putra, 05150 Alor Setar, Kedah, Malaysia
[2]Sabah Mineral Management, Block D, Unit 23A & 23, 5th Floor, Phase 1 KK Times Square, 88100 K. Kinabalu, Sabah, Malaysia
[3]Technical Service Division, Department of Mineral and Geoscience Malaysia, Jln Sultan Azlan Shah, 31400 Ipoh, Perak, Malaysia
[4]Department of Mineral and Geoscience Malaysia HQ, Level 9, Menara PjH, Jln Tun Abdul Razak, Precint 2, 62100 Putrajaya, Malaysia
[5]Department of Mineral and Geoscience Perak, Jln Sultan Azlan Shah, 31400 Ipoh, Perak, Malaysia
[6]Department of Mineral and Geoscience Selangor/W. Persekutuan, Level 6 & 7, Bangunan Darul Ehsan, Seksyen 14, 40000 Shah Alam, Selangor, Malaysia
*Corresponding author email address: afif@jmg.gov.my

Abstract: This paper reports on the rare earth element (REE) deposit in Bukit Enggang Granite in Sik, Kedah, and its enrichment patterns. The granitic rock in the study area is porphyritic biotite granite with K-feldspar, quartz and biotite as the main minerals, with randomly arranged K-feldspar phenocrysts. The average REE content in rock samples is 340.9 ppm. The exposed weathered profiles are between 3 to 7 meters in thickness. The C horizon is thicker than the B horizon. The average REE content in soil samples taken from the weathered profiles is 943.9 ppm. Interpretations from laboratory results reveal that the REE deposit in the study area is of the ion adsorption-type, with the REE enrichment in the weathered profiles originating from easily weathered REE bearing minerals in the parent rock, rather than highly resistant minerals like monazite, xenotime and zircon.

Keywords: REE, ion adsorption clay, Bukit Enggang, Kedah, monazite

Abstrak: Kertas ini membentangkan deposit unsur-unsur nadir bumi (REE) di Granit Bukit Enggang di Sik, Kedah, dan corak pengayaan yang wujud. Batuan granitik di kawasan kajian merupakan granit biotit porfiritik dengan K-feldspar, kuarza dan biotit sebagai mineral-mineral utama, dengan fenokris K-Feldspar yang bersusunan rawak. Kandungan purata REE dalam sampel-sampel batuan ialah 340.89 ppm. Profil luluhawa yang tersingkap menunjukkan ketebalan sekitar 3 hingga 7 meter, di mana horizon C adalah lebih tebal daripada horizon B. Kandungan purata REE dalam sampel-sampel tanih yang diambil daripada profil luluhawa ialah 943.85 ppm. Pentafsiran daripada keputusan makmal mendapati deposit REE di kawasan kajian ialah dari jenis jerapan ion, di mana pengayaan REE berasal daripada mineral-mineral kaya REE dalam batuan perumah yang mudah terluluhawa, berbanding mineral tahan luluhawa seperti monazit, zenotim dan zirkon.

Kata kunci: REE, lempung jerapan ion, Bukit Enggang, Kedah, monazit

INTRODUCTION

Background

Rare earth elements (REE) is in high demand worldwide in recent decades due to their uses in new technologies, especially in clean energy, consumer gadgets and the military sector. According to Hatch (2012) and Alonso *et al*. (2012), current demand of REE is consistently estimated to be 0.1 million tonnes in form of oxides, per annum.

REE consists of 17 chemical elements in the periodic table, comprising 15 lanthanides which are cerium (Ce), dysprosium (Dy), erbium (Er), europium (Eu), gadolinium (Gd), holmium (Ho), lanthanum (La), lutetium (Lu), neodymium (Nd), praseodymium (Pr), promethium (Pm), samarium (Sm), terbium (Tb), thulium (Tm) and ytterbium (Yb), as well as yttrium (Y) and scandium (Sc) (Connelly & Damhus, 2005). Although the REE are commonly found together naturally on earth's crust, each individual element has its own use. Pr, as for example, is in demand for producing nuclear batteries while La is needed to produce camera lenses and catalytic cracking catalysts.

REE mining from ion adsorption clays are not new to the world. Ion exchangeable REE in regolith-hosted deposits were first discovered in Longnan district, South China in the early 1970's (Neary & Highley, 1984). The enrichment of REE in weathered profiles are due to metamictization of REE rich minerals such as bastnaesite and fluoroapatite.

0126-6187; 2637-109X / Published by the Geological Society of Malaysia.

According to Sanematsu & Watanabe (2016), the term 'ion-adsorption type' could be used if the total REE content in a weathered profile is 50% greater than in the parent rock.

In comparison with other types of REE deposit, mining from the ion-adsorption type is regarded as environmentally friendly as it involves an in-situ leaching technique that produces relatively lower radioactive contamination than mining from other sources, such as in mineral form. Hence, REE sourced from ion-adsorption clays is also known as non-radioactive rare earth elements (NR-REE).

In Malaysia, NR-REE is classified as one of the Strategic Minerals in Malaysia, in addition to bauxite, tin, silica sand and kaolin. Resources are estimated in value at RM 747.2 billion (KeTSA, 2021).

Previous studies

The enrichment of REE in Malaysia is thought to be associated with tin bearing granites. Monazite and xenotime are REE containing accessory minerals that is commonly found in placer tin deposits.

Early studies on REE in Kedah focused on monazite and xenotime, from alluvial and placer deposits through panning in Jerai and Kulim (Willbourn, 1925; Flinter *et al*., 1963; Bradford, 1972; Wan Hassan, 1989). Teoh (1992) later studied rare earth minerals occurrences in the Sungai Tiang area, revealing that stream sediment concentrates from the Bukit Enggang area contained up to 24% monazite. A study by Mohd Hassan (1989) using quantitative mineral estimation (QME) analysis also revealed that streams flowing from the Bukit Enggang Granite contained sediments with high amount of zircon and rutile with minor occurrence of uranothorite.

Studies on REE as adsorbed ions in weathered granites commenced in 2013 by the Academy of Sciences Malaysia (ASM, 2014). In 2018, the Department of Mineral and Geoscience Malaysia (JMG) conducted a reconnaissance study on REE, including Th and Sc, in Malaysia. In Kedah, a preliminary study of clayey horizons in weathered granite throughout the state with a cut-off value of 300 ppm revealed several locations with high REE potential (Abdul Rahman *et al*., 2018; 2019; 2020). A reconnaissance study conducted by Fauzi (2018) revealed total REE contents in the weathered granite profiles of up to 706 ppm, prompting follow-up studies.

Hence, this paper aims to determine the type of REE deposit and its enrichment patterns in Bukit Enggang Granite.

Study area

The study area lies within the Bukit Enggang Forest Reserve, northeast of Sik town in Kedah with a total area of 1 km^2. The area contains an elongated ridge trending northeast-southwest with elevation ranging from 140 to 220 meters (Figure 1).

GEOLOGICAL SETTING

The study area is underlain by the Main Range Granite of Peninsular Malaysia, which is part of the Southeast Asian Magmatic Arc active during the Late Permian to Triassic subduction-collision event due to the closure of Paleo-Tethyan Ocean beneath the Indochina crust (Robb, 2019). The tin granites were the products of partial melting of the metamorphic basement during the collision of the Sibumasu and East Malaya blocks (Ng *et al.*, 2015; Liu *et al.*, 2020). The granite is characterized as S-type, peraluminous and ilmenite-series (Ishihara *et al*., 1979; Chappell & White, 2001). According to Yang *et al.* (2020), the genetic link between the tin mineralization and the granites has been constrained within the range of 220 to 210 Ma based on U-Th-Pb dating of cassiterite.

The granite in the study area, the Bukit Enggang Granite, is characterized as leucocratic, coarse-grained, and porphyritic with the principal minerals being quartz, alkali feldspar, plagioclase and biotite (Teoh, 1992). The granite lies adjacent to the Bukit Perak Granite to the northwest and the Rimba Telui Granite to the southeast, both being of similar Middle to Late Triassic age. The granites intruded older Paleozoic bedrock of the Mahang, Kubang Pasu and Semanggol formations.

MATERIALS AND METHODOLOGY

Soil and rock sampling

Soils developed on weathered granite were sampled for geochemistry in this study. The samples were collected in a grid, with a spacing of 200 meter between sample points, using a hand auger where no cut slopes were available. The soil samples were collected at a depth of 2 meter from the surface, within the B horizon. Samples from the C horizon, and the underlying bedrock (D horizon) were also taken, where possible, using the protocol of Husin *et al.* (2015), with slight modifications.

According to Wu *et al.* (1990), the B horizon is regarded as a zone in which the rock is completely weathered, containing approximately 30% clay, 35 – 40% quartz and 20 – 30% feldspar, readily disaggregated by hand, and sandy in texture, while in the the C horizon, the rock is only partially weathered, containing about 15-20% clay, and containing higher contents of mica, feldspar and quartz. Sanematsu *et al.* (2013) states that the B horizon rarely retains the original texture of the granite, while the lower C horizon shows remnants of granitic textures with the rock-forming minerals such as feldspars and biotite visible to the naked eye.

Soil samples were thoroughly dried in the shade at room temperature before disaggregation. The fraction used was that which passed through a 400 μm mesh. The sieved samples were separated into aliquots for X-ray fluorescence + Loss on ignition (XRF + LOI), Inductively Coupled Plasma Mass Spectrometry (ICP-MS) and X-ray diffraction (XRD) analysis. Rock samples were crushed to powder and subjected to the same analysis.

Geochemical analysis

Geochemical analysis was conducted using XRF and ICP-MS instruments, which are located in the Laboratory

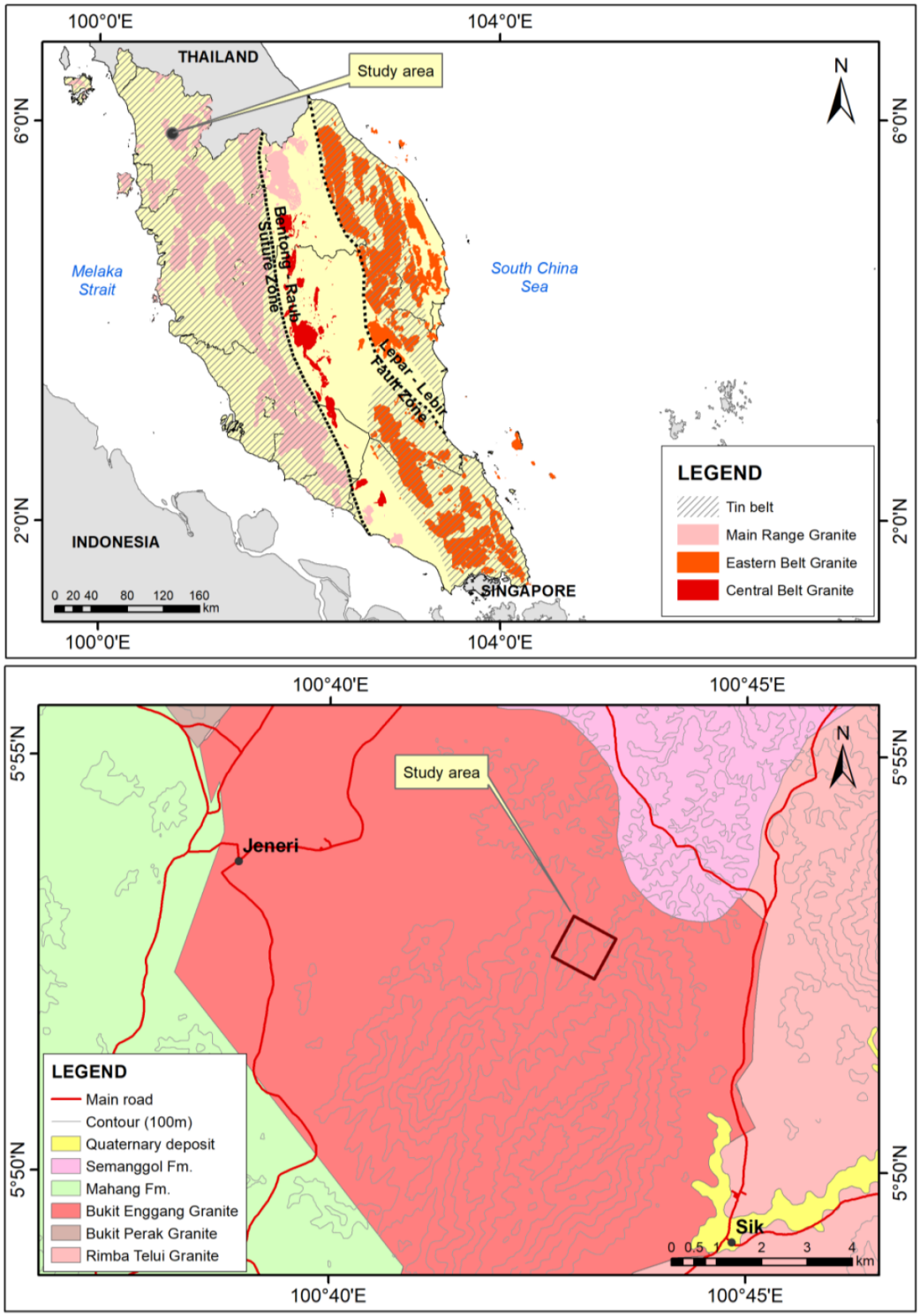

Figure 1: Maps showing the granite and tin belts in Peninsular Malaysia (top, after Hosking, 1973) and the general geology of study area (bottom, after JMG, 2014 and Teoh, 1992).

Branch, JMG Technical Service Division. The XRF analysis was conducted to obtain SiO_2, Al_2O_3, Fe_2O_3, TiO_2, Na_2O, K_2O, CaO, MgO, MnO, P_2O_5. The Loss on ignition (LOI) was obtained using standard analytical methods. REE, Th and U contents were obtained using ICP-MS. Total Light REE (TLREE), Total Heavy REE (THREE) and Total REE (TREE) values were calculated by summing the appropriate REE values. The minimum, maximum and average values of each element, TLREE, THREE and TREE were calculated, as well as the ratios Ce/Ce*, Eu/Eu* and La/Yb. Chondrite-normalized values were calculated using chondritic element abundances published in Suns & McDonough (1989) to produce the chondrite-normalized REE plots.

X-ray diffraction (XRD) analysis

The XRD analysis of selected soil and rock samples was conducted in the Mineralogy and Petrology Laboratory, JMG Technical Service Division. The analysis was conducted to identify clay minerals, and traces of Rare Earth-bearing minerals in the soil samples, and REE-bearing accessory minerals in the granite samples. Samples were ground to 25µm and loaded into standard XRD powder sample holders. Diffractograms were aquired between 0 and 60 degrees 2θ. Peaks were identified using Panalytical's Xpert Highscore Plus™ software, and quantification was conducted using the Highscore Plus Rietveldt Fitting module.

RESULTS

Field observation

The exposed weathered granite profiles in the study area range between 3 to 7 meters (Figure 2). The B horizon is generally slightly reddish to brownish and lacks feldspar, while the C horizon tends to be slightly yellowish or lighter than the upper horizons, and display relict granitic textures. The C horizon can be further divided into an upper C1 horizon and a lower C2 horizon, the latter containing less clay, and is looser, containing more relict feldspar. The depth of the B horizon varies between 2 and 5 meters, while the depth of C horizon is greater than 5 meters in most localities (Figure 3 and Figure 4).

The D horizon or granitic bedrock is not found within the study area. However, exposed granite boulders show phaneritic to porphyritic textures with randomly arranged K-feldspar phenocrysts, with quartz, K-feldspar and biotite as the main constituents (Figure 5).

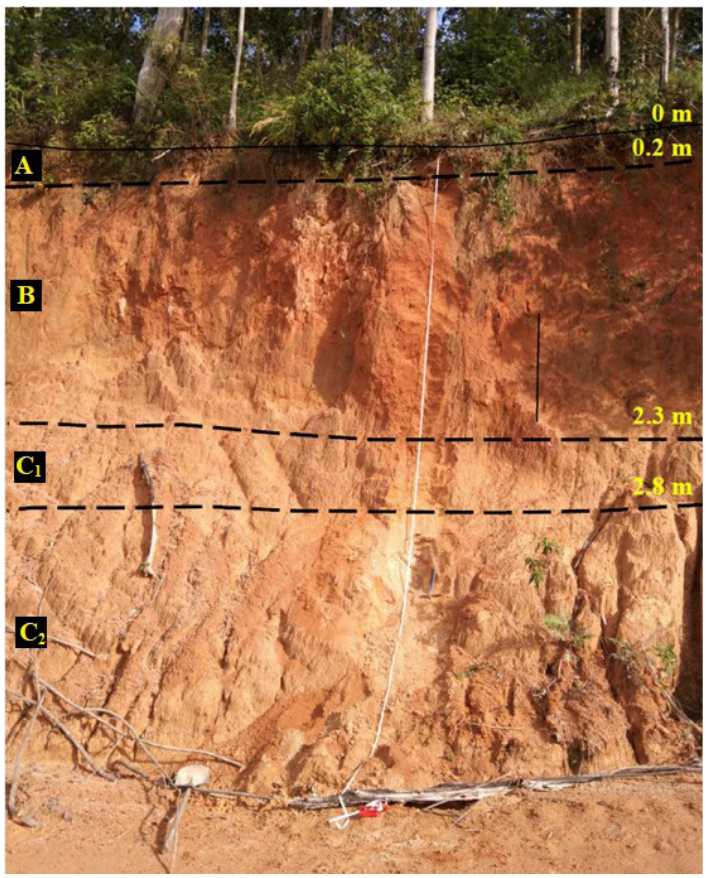

Figure 2: One of the exposed weathered granite profiles in Bukit Enggang area, showing A, B, C1 and C2 horizons.

Figure 3: Exposed B horizon showing reddish in colour with higher clay content and coarser quartz with grain size 2-4 mm.

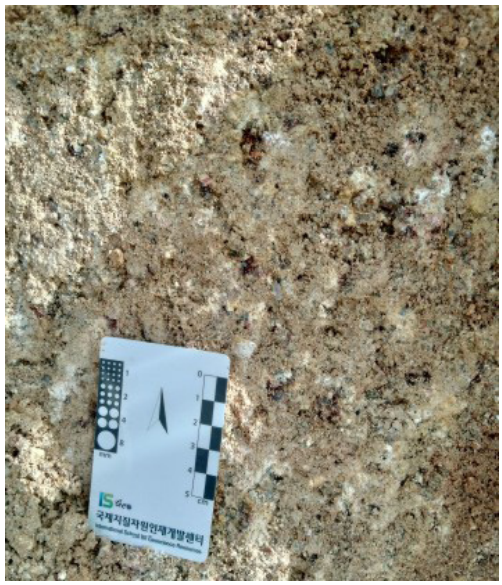

Figure 4: Exposed C1 horizon showing mottled, yellowish to brownish in colour with appearance of relict feldspar minerals and traces of biotite.

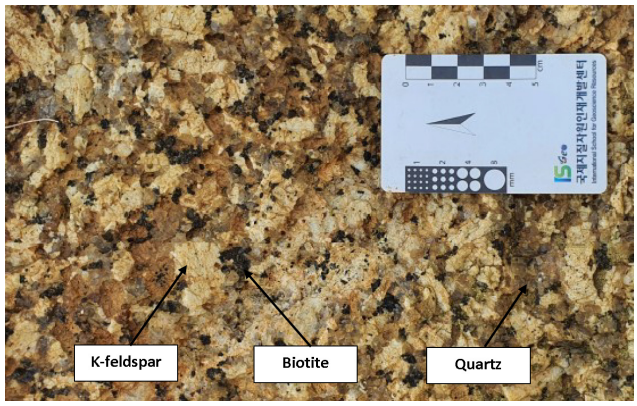

Figure 5: Exposed D horizon or bedrock showing phaneritic texture of biotite granite with white K-feldspar phenocryst.

XRF and LOI results

The XRF and LOI analysis of soil (Table 1) show high contents of SiO_2 (41.90 – 56.90%) and Al_2O_3 (23.50 – 34.60%) in all samples. The Fe_2O_3 content ranges from 1.53% to 6.53%, and K_2O content ranges from 0.52% to 9.10%. The CaO content is below detection in all samples, while the other oxides are less than 1%. LOI values range between 5.97% to 15.70%.

The XRF and LOI analyses of rock (Table 2) shows lower Al_2O_3 (12.50 – 17.00%) but higher SiO_2 (66.7 – 74.5%) and other oxides including Na_2O and K_2O, compared to the soil samples. The LOI values are very low, less than 2.28%.

ICP-MS results

The ICP-MS results for soil in Table 1 shows that TREE ranges from 432 to 1,455 ppm, with an average of 943 ppm. The bulk of this is TLREE (408.75 – 1,357.39 ppm), THREE being much lower (12.64 – 108.31 ppm). The soil sample KS1062 has the highest TREE, consisting of LREE elements, Gd, Tb, Er, Tm and Lu.

Th ranges between 109 ppm to 324 ppm, and U content ranges from 5.91 ppm to 33.36 ppm in soil (Table 1). KS1073 and KS1085 have the highest Th and U contents, respectively.

The ICP-MS results for rock in Table 2 shows that TREE ranges from 206.70 ppm to 475.07 ppm with an average of 340.89 ppm. As with soil, TLREE (159.48 – 390.99 ppm) is higher than THREE (47.22 – 84.08 ppm). Th and U in rock ranges between 47.30 ppm to 75.00 ppm and 6.18 ppm to 18.60 ppm, respectively.

The calculated Ce/Ce* and Eu/Eu* ratio values for soil samples lie between 1.98 to 2.81 and 0.02 to 0.12,

Table 1: Results of XRF, LOI and ICP-MS analysis of soil samples.

Sample	KS1051	KS1052	KS1053	KS1054	KS1055	KS1056	KS1057	KS1058	KS1059
Horizon	B	C	B	B	B	B	B	B	B
SiO_2	44.30	55.10	46.30	45.90	53.80	55.10	48.60	47.00	49.70
Al_2O_3	33.60	24.90	31.50	32.50	25.90	25.70	29.70	31.20	29.40
Fe_2O_3	3.88	2.70	4.46	5.30	3.65	3.61	4.32	4.54	4.05
TiO_2	0.45	0.31	0.39	0.46	0.54	0.60	0.62	0.52	0.41
Na_2O	0.08	0.32	0.12	0.07	0.26	0.15	0.13	0.13	0.16
K_2O	2.14	8.42	2.73	1.44	6.00	3.43	3.14	2.74	4.27
CaO	0.01	0.01	0.01	0.01	0.01	0.01	0.01	0.01	0.01
MgO	0.06	0.07	0.11	0.09	0.15	0.11	0.14	0.10	0.09
MnO	0.02	0.02	0.02	0.02	0.03	0.01	0.03	0.02	0.01
P_2O_5	0.03	0.03	0.03	0.03	0.05	0.04	0.06	0.03	0.03
LOI	14.30	7.24	13.20	13.20	8.81	10.30	12.40	12.80	11.00
Total	98.87	99.12	98.87	99.02	99.2	99.06	99.15	99.09	99.13
Sc	15.09	8.84	13.99	15.23	10.26	10.31	13.91	18.18	11.79
Y	9.99	10.00	25.58	22.10	45.90	11.49	23.68	35.21	13.92
La	49.63	44.44	102.47	93.03	194.82	39.49	180.35	123.39	69.71
Ce	622.60	361.39	443.97	721.81	338.90	304.17	547.96	499.56	379.54
Pr	9.25	10.13	27.81	23.32	44.41	11.14	41.64	38.10	16.73
Nd	31.46	35.31	95.74	78.24	153.28	37.05	142.44	130.94	55.53
Sm	7.77	7.24	18.61	15.51	29.55	6.60	25.97	23.94	10.61
Eu	0.25	0.54	0.37	0.25	1.25	0.25	0.61	1.24	0.25
Gd	6.19	5.31	12.10	10.78	20.06	4.31	16.56	15.74	7.16
Tb	0.50	0.46	1.26	1.13	2.36	0.49	1.66	1.89	0.74
Dy	2.52	2.35	6.37	5.67	11.88	2.68	7.19	9.61	3.65
Ho	0.34	0.31	1.00	0.86	1.89	0.41	0.97	1.48	0.50
Er	1.11	1.12	2.83	2.41	4.89	1.44	2.48	3.92	1.44
Tm	0.08	0.09	0.32	0.25	0.59	0.15	0.25	0.46	0.12
Yb	1.89	1.77	3.91	3.32	6.41	2.47	3.92	5.30	2.48
Lu	0.10	0.10	0.28	0.23	0.49	0.16	0.21	0.35	0.11
Th	183.90	162.28	179.82	212.03	178.82	177.66	216.29	224.38	197.95
U	9.19	10.22	18.77	17.11	23.61	16.40	16.69	19.14	14.51
TLREE	736.05	467.89	702.96	947.39	772.47	409.01	952.88	835.35	544.16
THREE	22.72	21.51	53.65	46.75	94.47	23.60	56.92	73.96	30.12
TREE	758.77	489.40	756.61	994.14	866.94	432.61	1009.80	909.31	574.28
Ce/Ce*	21.15	13.24	6.82	12.41	2.83	12.02	4.94	6.19	8.78
Eu/Eu*	0.04	0.09	0.02	0.02	0.05	0.05	0.03	0.06	0.03
La/Yb	26.26	25.14	26.21	28.05	30.38	15.97	46.03	23.30	28.14

Ce/Ce* $Ce_N/(La_N \times Pr_N)^{1/2}$, Eu/Eu* $Eu_N/(Sm_N \times Gd_N)^{1/2}$ (where N is normalized by C1-chondrite (Sun & McDonough, 1989)).

Table 1 (cont.): Results of XRF, LOI and ICP-MS analysis of soil samples.

Sample	KS1060	KS1061	KS1062	KS1063	KS1064	KS1065	KS1066	KS1067	KS1068
Horizon	C	B	B	C	B	B	B	B	B
SiO_2	52.60	45.90	51.70	53.90	53.20	45.30	49.90	46.20	41.90
Al_2O_3	27.10	32.70	26.00	26.10	26.90	32.50	28.28	31.40	34.60
Fe_2O_3	3.57	4.79	6.53	3.43	1.53	4.92	4.21	4.98	5.55
TiO_2	0.41	0.57	0.37	0.35	0.36	0.59	0.56	0.42	0.43
Na_2O	0.23	0.06	0.14	0.25	0.14	0.05	0.10	0.10	0.03
K_2O	6.38	1.24	4.45	6.71	3.78	1.05	2.92	2.31	0.73
CaO	0.01	0.01	0.01	0.01	0.01	0.01	0.01	0.01	0.01
MgO	0.11	0.09	0.10	0.08	0.06	0.07	0.06	0.08	0.06
MnO	0.02	0.03	0.02	0.02	0.02	0.03	0.02	0.01	0.02
P_2O_5	0.03	0.04	0.04	0.03	0.03	0.05	0.04	0.03	0.04
LOI	8.81	13.80	9.89	8.48	10.80	14.30	12.40	13.70	15.70
Total	99.27	99.23	99.25	99.36	96.83	98.87	98.50	99.24	99.07
Sc	13.32	15.04	8.30	11.25	10.31	12.39	10.38	12.09	15.42
Y	20.68	15.04	46.50	19.41	14.12	19.13	10.61	18.41	6.93
La	104.20	104.38	280.12	107.15	37.00	102.57	70.31	95.33	44.95
Ce	440.94	516.85	789.28	351.38	315.48	577.39	414.08	450.32	634.43
Pr	20.12	30.74	57.27	28.85	11.81	27.04	17.68	23.85	9.86
Nd	68.30	101.19	185.33	99.51	42.67	87.44	56.56	78.01	31.35
Sm	12.82	16.34	35.19	18.02	8.82	16.47	9.37	13.41	5.82
Eu	0.91	0.25	1.90	0.95	0.25	0.25	0.25	0.25	0.25
Gd	10.79	10.94	21.57	11.46	5.74	11.29	6.46	9.25	4.61
Tb	0.85	1.03	2.26	1.11	0.64	1.18	0.59	0.96	0.34
Dy	4.21	4.56	11.58	5.52	3.41	5.59	2.82	4.62	1.80
Ho	0.58	0.57	1.90	0.80	0.52	0.78	0.35	0.67	0.16
Er	1.61	1.48	5.41	2.24	1.73	2.14	1.12	1.77	0.60
Tm	0.15	0.11	0.70	0.24	0.19	0.20	0.08	0.15	0.05
Yb	2.36	2.63	7.43	3.59	2.98	3.36	2.18	2.72	1.39
Lu	0.12	0.09	0.62	0.20	0.20	0.17	0.07	0.11	0.01
Th	122.65	256.90	164.17	129.92	273.86	208.93	212.42	236.05	229.13
U	15.90	15.38	14.46	24.46	21.05	20.16	20.68	13.45	10.88
TLREE	660.61	784.79	1357.39	617.11	426.34	823.55	578.63	673.26	742.08
THREE	41.35	36.45	97.97	44.57	29.53	43.84	24.28	38.66	15.89
TREE	701.96	821.24	1455.36	661.68	455.87	867.39	602.91	711.92	757.97
Ce/Ce*	7.09	7.65	4.68	5.17	12.93	8.91	9.41	7.56	23.15
Eu/Eu*	0.08	0.02	0.07	0.06	0.03	0.02	0.03	0.02	0.05
La/Yb	44.21	39.76	37.71	29.84	12.42	30.51	32.25	35.03	32.38

Table 1 (cont.): Results of XRF, LOI and ICP-MS analysis of soil samples.

Sample	KS1069	KS1070	KS1071	KS1072	KS1073	KS1074	KS1075	KS1076	KS1077
Horizon	B	B	B	C	B	C	B	B	C
SiO_2	50.70	45.00	46.90	51.70	53.90	55.80	54.20	49.00	55.90
Al_2O_3	29.20	33.20	30.80	27.30	25.20	24.90	26.10	30.30	25.20
Fe_2O_3	3.60	5.01	4.85	3.67	3.88	2.46	3.34	4.13	2.50
TiO_2	0.35	0.45	0.43	0.25	0.61	0.65	0.76	0.42	0.26
Na_2O	0.10	0.03	0.12	0.25	0.27	0.29	0.10	0.10	0.29
K_2O	2.59	0.73	3.24	6.91	5.99	7.06	2.44	3.10	7.79
CaO	0.01	0.01	0.01	0.01	0.01	0.01	0.01	0.01	0.01
MgO	0.07	0.05	0.14	0.11	0.24	0.28	0.10	0.19	0.10
MnO	0.02	0.01	0.01	0.01	0.03	0.02	0.04	0.02	0.02
P_2O_5	0.03	0.03	0.03	0.03	0.05	0.03	0.04	0.04	0.04
LOI	12.50	14.60	12.70	9.06	8.91	7.58	11.20	11.90	7.17
Total	99.17	99.12	99.23	99.3	99.09	99.08	98.33	99.21	99.28
Sc	10.35	15.16	12.79	10.78	25.72	10.77	10.77	12.40	6.99
Y	12.55	5.73	20.53	16.42	44.49	36.52	17.88	27.86	41.20
La	37.41	30.49	72.07	62.09	202.54	158.85	95.40	159.16	198.21
Ce	328.43	376.66	348.60	278.87	715.94	193.93	533.58	470.16	268.40
Pr	11.78	7.76	21.52	17.94	42.52	36.70	21.09	43.68	50.17
Nd	41.50	24.49	72.12	60.43	143.00	119.94	68.99	147.66	167.31
Sm	9.45	4.39	13.85	10.78	34.08	21.74	15.01	27.48	33.49
Eu	0.25	0.25	0.83	1.06	1.40	1.25	0.44	0.97	1.78
Gd	5.64	2.84	8.29	7.12	19.81	14.52	9.72	15.13	20.51
Tb	0.65	0.29	1.06	0.82	2.45	1.57	1.03	1.54	2.23
Dy	3.16	1.72	5.54	4.35	11.88	7.88	4.97	7.46	10.50
Ho	0.41	0.16	0.84	0.61	1.93	1.28	0.68	1.11	1.63
Er	1.34	0.67	2.42	1.77	5.15	3.48	1.89	3.10	4.30
Tm	0.12	0.05	0.26	0.17	0.65	0.42	0.21	0.37	0.51
Yb	2.10	1.20	3.25	2.55	8.19	5.03	3.15	4.92	6.05
Lu	0.12	0.03	0.24	0.14	0.62	0.34	0.19	0.32	0.42
Th	271.80	203.77	224.90	177.22	324.41	138.93	201.78	210.53	131.76
U	11.76	10.68	16.44	13.52	25.95	13.66	14.79	12.22	9.61
TLREE	439.17	459.20	541.78	441.95	1165.20	543.18	745.28	861.51	726.35
THREE	26.09	12.69	42.43	33.95	95.17	71.04	39.72	61.81	87.35
TREE	465.26	471.89	584.21	475.90	1260.37	614.22	785.00	923.32	813.70
Ce/Ce*	13.35	19.69	7.45	6.97	5.84	1.98	9.16	4.64	2.16
Eu/Eu*	0.03	0.07	0.08	0.12	0.05	0.07	0.04	0.05	0.07
La/Yb	17.85	25.46	22.17	24.33	24.74	31.58	30.32	32.33	32.75

Table 1 (cont.): Results of XRF, LOI and ICP-MS analysis of soil samples.

Sample	KS1078	KS1079	KS1080	KS1081	KS1082	KS1083	KS1084	KS1085
Horizon	**B**	**C**	**B**	**C**	**B**	**B**	**C**	**C**
SiO_2	46.50	50.90	44.90	51.30	49.10	50.60	54.80	56.90
Al_2O_3	31.40	28.50	33.60	28.50	28.90	28.50	25.20	23.50
Fe_2O_3	4.52	3.51	4.52	3.56	4.20	3.36	3.37	2.52
TiO_2	0.51	0.46	0.43	0.46	0.49	0.66	0.51	0.34
Na_2O	0.13	0.22	0.03	0.24	0.17	0.12	0.26	0.34
K_2O	2.87	5.56	0.52	5.46	4.78	3.13	7.27	9.10
CaO	0.01	0.01	0.01	0.01	0.01	0.01	0.01	0.01
MgO	0.13	0.15	0.07	0.12	0.19	0.14	0.17	0.16
MnO	0.03	0.03	0.01	0.02	0.02	0.04	0.03	0.02
P_2O_5	0.05	0.03	0.03	0.03	0.03	0.05	0.04	0.07
LOI	12.80	9.92	14.80	9.45	11.10	12.20	7.43	5.97
Total	98.95	99.29	98.92	99.15	98.99	98.81	99.09	92.96
Sc	19.73	11.70	14.43	16.04	13.72	14.74	10.55	3.48
Y	32.85	24.37	6.51	9.06	65.71	37.52	32.59	15.12
La	186.46	152.74	30.19	66.19	166.82	154.39	138.59	124.57
Ce	748.62	457.52	516.89	593.46	749.97	657.19	333.92	268.36
Pr	35.12	39.53	6.72	15.63	29.38	42.55	36.98	46.97
Nd	119.47	135.72	25.96	58.17	102.56	150.08	131.56	133.53
Sm	24.62	26.49	4.29	8.60	17.53	24.82	21.61	17.62
Eu	1.20	1.48	0.30	0.76	0.99	1.38	1.45	0.98
Gd	20.18	15.41	3.47	6.10	17.55	17.26	14.62	14.33
Tb	1.51	1.62	0.29	0.47	1.83	1.89	1.67	1.38
Dy	7.14	7.58	1.88	2.51	9.74	9.08	8.31	5.29
Ho	0.99	1.05	0.20	0.30	1.79	1.43	1.27	0.82
Er	2.59	2.74	0.67	0.91	5.03	3.77	3.30	1.86
Tm	0.27	0.30	0.05	0.06	0.62	0.44	0.37	0.47
Yb	3.91	4.44	1.26	1.70	5.49	4.49	4.02	4.15
Lu	0.23	0.25	0.05	0.08	0.55	0.40	0.32	0.48
Th	206.84	140.84	178.52	109.25	181.32	196.42	135.04	158.14
U	20.26	17.34	5.91	10.90	13.20	15.93	18.04	33.36
TLREE	1135.22	825.18	598.78	758.85	1080.97	1045.15	674.66	595.51
THREE	69.67	57.76	14.38	21.19	108.31	76.28	66.47	43.90
TREE	1204.89	882.94	613.16	780.04	1189.28	1121.43	741.13	639.41
Ce/Ce*	6.76	4.76	28.01	14.51	7.64	6.67	3.80	3.13
Eu/Eu*	0.05	0.07	0.08	0.10	0.06	0.07	0.08	0.06
La/Yb	47.73	34.43	23.97	39.01	30.38	34.40	34.51	30.01

Table 2: Results of XRF, LOI and ICP-MS analysis of rock samples.

Sample	KR1051	KR1052	KR1053	KR1054
Rock type	Biotite granite	Biotite granite	Biotite granite	Biotite granite
SiO_2	74.50	74.10	71.60	66.70
Al_2O_3	12.50	12.90	14.20	17.00
Fe_2O_3	2.14	1.76	2.46	2.25
TiO_2	0.23	0.23	0.35	0.33
Na_2O	2.34	2.67	2.08	3.74
K_2O	5.79	5.74	5.67	7.34
CaO	0.63	0.88	0.42	0.25
MgO	0.30	0.24	0.34	0.30
MnO	0.03	0.03	0.04	0.02
P_2O_5	0.07	0.06	0.06	0.06
LOI	0.65	0.51	2.28	1.53
Total	99.18	99.12	99.50	97.90
Sc	3.04	4.29	4.83	2.71
Y	34.40	27.20	49.10	30.70
La	57.50	37.80	100.00	55.60
Ce	108.00	76.60	171.00	83.00
Pr	11.30	8.05	22.80	17.90
Nd	41.10	27.10	75.10	44.10
Sm	8.26	4.92	16.70	8.74
Eu	0.21	0.72	0.56	0.35
Gd	6.05	6.34	12.30	6.63
Tb	1.01	1.05	1.78	1.00
Dy	5.14	6.48	9.36	5.54
Ho	1.04	0.52	1.67	0.99
Er	3.01	2.14	4.51	2.81
Tm	0.43	0.31	0.58	0.37
Yb	3.32	2.71	4.13	3.07
Lu	0.55	0.47	0.65	0.51
Th	63.50	47.30	75.00	52.30
U	11.90	13.40	18.60	6.18
TLREE	229.41	159.48	390.99	212.40
THREE	54.95	47.22	84.08	51.62
TREE	284.36	206.70	475.07	264.02
Ce/Ce*	3.14	3.34	2.79	2.26
Eu/Eu*	0.03	0.13	0.04	0.05
La/Yb	17.32	13.95	24.21	18.11

Ce/Ce* $Ce_N/(La_N \times Pr_N)^{1/2}$, Eu/Eu* $Eu_N/(Sm_N \times Gd_N)^{1/2}$ (where N is normalized by C1-chondrite (Sun & McDonough, 1989)).

Table 3: Results of XRD analysis of selected soil samples. The symbol '-' denotes not detected and 'Tr' denotes trace.

Sample	KS 1051	KS 1052	KS 1062	KS 1063	KS 1071	KS 1072	KS 1073	KS 1074	KS 1076	KS 1077	KS 1078	KS 1079	KS 1080	KS 1081
Horizon	**B**	**C**	**B**	**C**	**B**	**C**	**B**	**C**	**B**	**C**	**B**	**C**	**B**	**C**
Kaolinite	98	62	97	49	99	62	95	95	98	78	98	98	100	79
Gibbsite	-	9	-	-	-	-	-	-	-	-	-	-	-	-
Monazite	Tr	-	Tr	-	Tr	Tr	-	1	Tr	1	Tr	Tr	-	Tr
Xenotime	Tr	Tr	Tr	-	Tr	-	1	1	-	Tr	Tr	1	-	Tr
Zircon	1	1	1	-	1	Tr	1	Tr	1	1	-	1	-	-
Feldspar	1	-	2	41	-	30	2	3	-	2	2	-	Tr	21
Rutile	-	6	-	-	-	-	1	-	-	-	-	-	-	-
Biotite	-	16	-	-	-	-	-	-	-	-	-	-	-	-
Clinochlore	-	6	-	-	-	-	-	-	-	-	-	-	-	-
Mica	-	-	-	4	-	-	-	-	-	-	-	-	-	-
Quartz	-	-	Tr	6	-	8	-	-	1	19	-	-	Tr	-
Total	100	100	100	100	100	100	100	100	100	100	100	100	100	100

respectively, while the La/Yb ratio values range between 12.42 to 47.73 (Table 1). As for rock samples, the calculated Ce/Ce* and Eu/Eu* values lie between 2.26 to 3.34 and 0.03 to 0.13 respectively, while the La/Yb ratio values range between 13.95 to 24.21 (Table 2).

XRD results

Bulk powder XRD analysis shows that all soil samples contain kaolinite (more than 49%) as the only clay mineral, while sample KS1052 contains low gibbsite content (Table 3). REMs like monazite, xenotime and zircon are detected in almost all soil samples with contents no greater than 1.2%. Feldspar, particularly K-feldspar, and quartz are the main non-clay minerals detected in almost all samples, while biotite and mica appear in several samples in very low amount. Rutile, clinochlore and ilmenite are also detected in some soil samples.

Bulk powder XRD analyses of rock samples detected quartz and feldspars as the main constituent minerals, while biotite, apatite, ilmenite, rutile and kaolinite appear in some of the samples (Table 4). Monazite and other REMs are not detected in any of the rock samples. Selected soil and rock XRD diffractograms are shown in Figures 6, 7 and 8.

Major oxides, LOI and elements correlation coefficients

Pearson's Correlation Coefficients are shown as a matrix in Table 5 and the selected correlation plots are shown in Figure 9. Strong, positive relationships are shown by SiO_2-Na_2O, SiO_2-K_2O, Al_2O_3-Fe_2O_3, Al_2O_3-LOI, Fe_2O_3-LOI, Fe_2O_3-Ce and TiO_2-MnO.

Na_2O has strong, positive relationships with K_2O and MgO. MgO also has strong, positive relationships with all REE except Sc and Ce, while MnO only shows strong, positive relationships with Nd, Sm, Gd and Tb. P_2O_5 shows strong, positive relationships with MnO, Pr, Nd and U. Eu has strong, positive relationships with both Na_2O and K_2O.

Y also has strong, positive relationships with all REE except Sc and Ce, while Th is only strongly correlated with LOI.

Table 4: Results of XRD analysis of rock samples. The symbol '-' denotes not detected and 'Tr' denotes trace.

	KR1051	KR1052	KR1053	KR1054
Quartz	40	32	18	41
Orthoclase	14	26	7	21
Albite	-	30	37	33
Microcline	36	9	35	-
Biotite	10	3	3	3
Mica	-	-	-	-
Apatite	-	-	-	1
Ilmenite	-	-	1	-
Rutile	-	-	Tr	-
Magnetite	-	-	-	-
Hematite	-	-	-	-
Kaolinite	-	-	1	1
Gibbsite	-	-	-	-
Monazite	-	-	-	-
	100	100	100	100

Chondrite-normalized REE plot

The chondrite-normalized REE plot for soil (Figure 10) shows that all samples have negative Eu and positive Yb anomalies. Only samples KS1074, KS1077 and KS1085

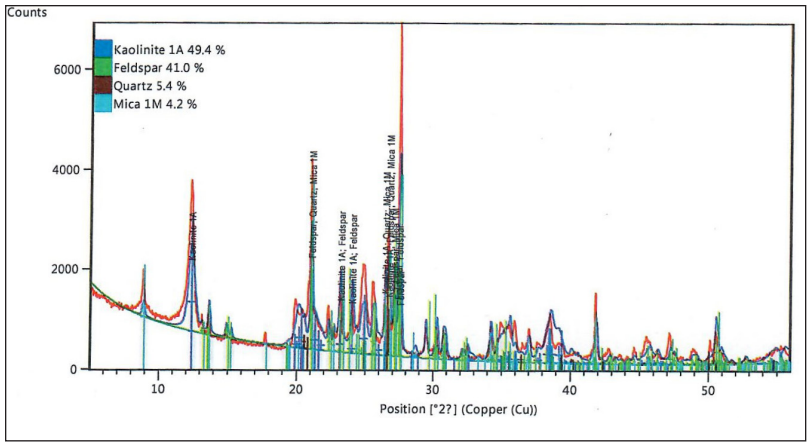

Figure 6: XRD diffractogram of soil sample KS1063.

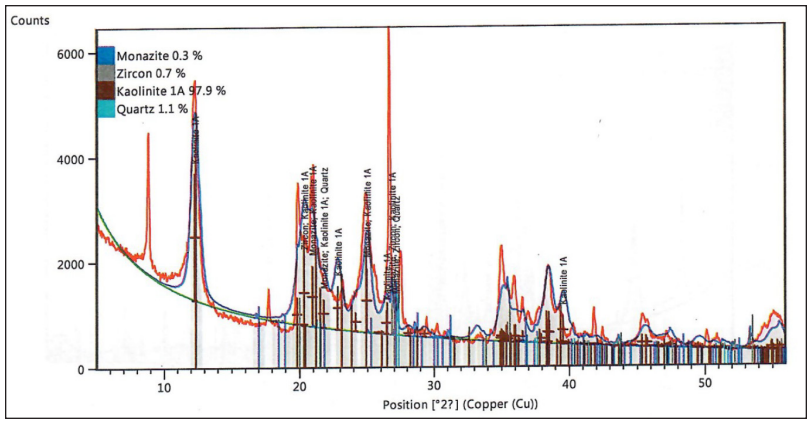

Figure 7: XRD diffractogram of soil sample KS1076.

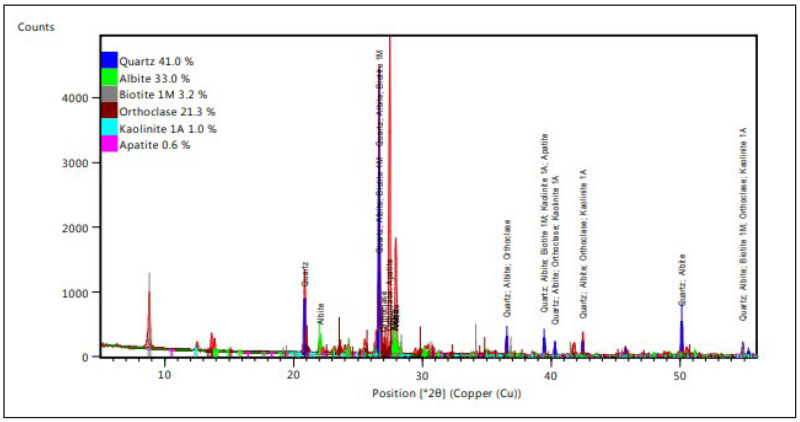

Figure 8: XRD diffractogram of rock sample KR1053.

Table 5: Pearson's correlation coefficients for major oxides, REE, Th and U of soil samples. The bolded value denotes strong relationship.

	SiO_2	Al_2O_3	Fe_2O_3	TiO_2	Na_2O	K_2O	MgO	MnO	P_2O_5	LOI	Sc	Y	La	Ce	Pr	Nd
SiO_2	**1.00**	-0.98	-0.73	-0.04	**0.84**	**0.84**	0.42	0.17	0.21	-0.93	-0.49	0.26	0.29	-0.49	0.34	0.33
Al_2O_3		**1.00**	**0.65**	0.04	-0.85	-0.86	-0.45	-0.18	-0.25	**0.94**	0.47	-0.33	-0.36	0.42	-0.40	-0.38
Fe_2O_3			**1.00**	0.08	-0.64	-0.63	-0.25	-0.15	-0.05	**0.65**	0.36	0.02	0.12	**0.60**	0.01	0.01
TiO_2				**1.00**	-0.25	-0.32	0.35	**0.60**	0.33	0.21	0.37	0.19	0.19	0.30	0.14	0.16
Na_2O					**1.00**	**0.98**	**0.51**	0.07	0.16	-0.96	-0.33	0.32	0.34	-0.42	0.39	0.38
K_2O						**1.00**	0.47	0.04	0.14	-0.97	-0.42	0.31	0.34	-0.44	0.39	0.38
MgO							**1.00**	0.27	0.28	-0.48	0.15	**0.64**	**0.59**	-0.01	**0.59**	**0.59**
MnO								**1.00**	**0.51**	-0.10	0.18	0.36	0.48	0.36	0.48	**0.50**
P_2O_5									**1.00**	-0.17	-0.08	0.20	0.46	0.14	**0.55**	**0.51**
LOI										**1.00**	**0.45**	-0.32	-0.36	0.45	-0.41	-0.40
Sc											**1.00**	0.13	0.05	**0.61**	-0.09	-0.04
Y												**1.00**	**0.84**	0.31	**0.74**	**0.77**
La													**1.00**	0.34	**0.93**	**0.94**
Ce														**1.00**	0.15	0.17
Pr															**1.00**	**0.99**
Nd																**1.00**

Table 5 (cont.): Pearson's correlation coefficients for major oxides, REE, Th and U of soil samples. The bolded value denotes strong relationship.

	Sm	Eu	Gd	Tb	Dy	Ho	Er	Tm	Yb	Lu	Th	U	TLREE	THREE	TREE
SiO_2	0.31	0.49	0.28	0.33	0.31	0.33	0.32	0.40	0.38	0.44	-0.36	0.35	-0.17	0.30	-0.13
Al_2O_3	-0.36	-0.54	-0.35	-0.39	-0.38	-0.40	-0.39	-0.48	-0.45	-0.51	0.34	-0.41	0.09	-0.37	0.04
Fe_2O_3	0.03	-0.15	0.02	-0.01	0.03	0.01	0.03	-0.03	-0.01	-0.07	0.23	-0.20	0.46	0.02	0.42
TiO_2	0.17	-0.05	0.19	0.21	0.20	0.18	0.17	0.11	0.16	0.10	0.22	0.15	0.31	0.19	0.31
Na_2O	0.35	**0.60**	0.37	0.39	0.36	0.38	0.35	0.43	0.40	0.45	-0.48	**0.37**	-0.10	0.36	-0.05
K_2O	0.33	**0.61**	0.35	0.36	0.34	0.36	0.34	0.42	0.38	0.44	-0.52	0.33	-0.11	0.34	-0.07
MgO	**0.58**	**0.59**	**0.60**	**0.63**	**0.63**	0.64	**0.62**	**0.65**	**0.65**	**0.65**	-0.10	0.28	0.33	**0.65**	0.37
MnO	**0.52**	0.32	**0.54**	**0.50**	0.46	0.41	0.37	0.33	0.39	0.33	0.08	0.32	**0.53**	0.43	**0.54**
P_2O_5	0.44	0.24	**0.49**	0.44	0.35	0.31	0.25	0.37	0.37	0.41	0.13	**0.58**	0.37	0.31	0.37
LOI	-0.36	-0.60	-0.36	-0.38	-0.36	-0.38	-0.36	-0.45	-0.41	-0.48	**0.50**	-0.35	0.10	-0.36	0.06
Sc	0.09	-0.05	0.09	0.08	0.11	0.09	0.10	-0.01	0.09	-0.02	**0.47**	-0.04	0.44	0.11	**0.42**
Y	**0.80**	**0.74**	**0.87**	**0.89**	**0.93**	**0.95**	**0.96**	**0.91**	**0.88**	**0.88**	-0.05	0.21	**0.67**	**0.98**	**0.72**
La	**0.95**	**0.81**	**0.97**	**0.93**	**0.92**	**0.89**	**0.88**	**0.86**	**0.90**	**0.83**	-0.12	0.31	**0.78**	**0.91**	**0.82**
Ce	0.23	0.06	0.30	0.22	0.24	0.24	0.25	0.19	0.22	0.21	0.25	-0.09	**0.84**	0.29	**0.81**
Pr	**0.95**	**0.80**	**0.94**	**0.93**	**0.89**	**0.86**	**0.82**	**0.85**	**0.87**	**0.82**	-0.13	0.44	**0.65**	**0.85**	**0.68**
Nd	**0.97**	**0.82**	**0.95**	**0.95**	**0.91**	**0.88**	**0.84**	**0.85**	**0.88**	**0.82**	-0.13	0.40	**0.66**	**0.87**	**0.70**
Sm	**1.00**	**0.81**	**0.96**	**0.96**	**0.94**	**0.90**	**0.88**	**0.85**	**0.93**	**0.82**	-0.03	0.36	**0.70**	**0.89**	**0.74**
Eu		**1.00**	**0.81**	**0.81**	**0.81**	**0.80**	**0.78**	**0.79**	**0.78**	**0.76**	-0.36	0.21	**0.50**	**0.79**	**0.55**
Gd			**1.00**	**0.97**	**0.95**	**0.92**	**0.89**	**0.88**	**0.91**	**0.85**	-0.09	0.39	**0.75**	**0.94**	**0.79**
Tb				**1.00**	**0.99**	**0.98**	**0.95**	**0.93**	**0.96**	**0.90**	-0.01	0.40	**0.68**	**0.96**	**0.73**

Table 5 (cont.): Pearson's correlation coefficients for major oxides, REE, Th and U of soil samples. The bolded value denotes strong relationship.

	Dy	Ho	Er	Tm	Yb	Lu	Th	U	TLREE	THREE	TREE
Dy	**1.00**	**0.99**	**0.98**	**0.94**	**0.96**	**0.91**	-0.01	0.35	**0.68**	**0.98**	**0.73**
Ho		**1.00**	**0.99**	**0.97**	**0.97**	**0.94**	-0.02	0.34	**0.67**	**0.99**	**0.72**
Er			**1.00**	**0.96**	**0.96**	**0.93**	0.00	0.30	**0.66**	**0.98**	**0.71**
Tm				**1.00**	**0.96**	**0.99**	-0.03	0.41	**0.62**	**0.95**	**0.67**
Yb					**1.00**	**0.95**	0.06	0.42	**0.66**	**0.94**	**0.70**
Lu						**1.00**	-0.01	0.45	**0.61**	**0.91**	**0.66**
Th							**1.00**	0.14	0.11	-0.04	0.10
U								**1.00**	0.14	0.30	0.16
TLREE									**1.00**	**0.71**	**1.00**
THREE										**1.00**	**0.76**
TREE											**1.00**

show slightly negative Ce anomalies while sample KS1085 shows a slightly positive Tm anomaly, compared to others. All rock samples show negative anomalies for both Ce and Eu.

DISCUSSION

Clay minerals from granite weathering

Higher Al_2O_3 and LOI and lower Na_2O and K_2O values in soil when compared to rock indicate weathering process that convert K-feldspars (microcline/orthoclase/sanidine) or Na-rich plagioclase feldspar (albite) to clay minerals, particularly kaolinites, which are detected in all soil samples via XRD analysis:

$$3KAlSi_3O_8 + 2H^+ + 9H_2O \rightarrow Al_2Si_2O_5(OH)_4 + 3K^+ + 4H_4SiO_4$$
(K-feldspar) (Kaolinite)

$$NaAlSi_3O_8 + 2H^+ + 9H_2O \rightarrow Al_2Si_2O_5(OH)_4 + Na^+ + 4H_4SiO_4$$
(Albite) (Kaolinite)

C horizon samples, except KS1063 and KS1085, have lower Al_2O_3 and LOI values than those in corresponding upper horizons. This confirms that the weathering processes that produced clay minerals occurred mainly in the B horizon.

This is consistent the result of studies of biotite-K-feldspar granite in Zudong and Guanxi, China, which found a positive correlation between Al_2O_3 and LOI exists, which corresponds with the progression from unaltered bedrock to increasingly weathered zones (Wu *et al.*, 1990).

All rock samples contain more K_2O than Na_2O. This is also true for all soil samples, indicating that the kaolinite in the soil was derived from K-rich feldspars in the rock. Anorthite is almost absent in the local granite and is unlikely to be the progenitor of the clay minerals in the soil, and for this reason CaO contents are low (<0.88%) in all soil and rock samples.

REE origin, transport and accumulation

Monazite, one of the main REE-bearing minerals (REM) found in granite, has been detected by XRD analysis in soil. Monazite, zircon and xenotime, are an unlikely sources for REE, as these minerals are refractory and are resistant to weathering (Sengupta & Van Gosen, 2016; Zhou *et al.*, 2017). More likely sources for the REE in the soil would be soluble REMs such as apatite, and silicate minerals such as allanite and titanite (sphene) (Bao & Zhao, 2008; Ishihara *et al.*, 2008). Fluorocarbonate minerals can be found crystallizing in cavities and along boundaries or fractures in feldspars, as seen in the Phuket Granite (Sanematsu *et al*., 2011), while allanite, parasite, bastnaesite and monazite appear as inclusions in biotite and / or plagioclase as reported in the Bangka Islands (Tampubolon *et al*., 2022). Apatite was also detected in rock sample KR1054.

In this study, positively charged REE ions released from REMs due to weathering are transported downward and adsorbed by clay minerals, mostly kaolinites, in lower horizon where the pH condition is less acidic. The weathering of REE from REMs in near surface horizons is triggered by acidic soil water due to the presence of humic substances and atmospheric CO_2 (Sanematsu *et al.*, 2013).

Higher REE contents in the clayey B and C horizons than in the rock confirms ion-adsorption enrichment in these horizons. Sanematsu *et al.* (2013) suggests that the B horizon acts as a REE accumulation zone, the source being REE leached from overlying near-surface horizons where acidic and oxidation conditions prevail.

Kaolinite, along with halloysite and/or Fe and Al hydroxides were identified as adsorptive minerals in ion-adsorption type REE deposits in southern China (Wu *et al.*, 1990; Bao & Zhao, 2008). Gibbsite is also a possible REE adsorber, due to its disordered structure (Aubert *et al.*, 2000; Abdul Rahman, 2011). It has a higher Cation Exchange Capacity (CEC) than kaolinite, and is potentially a better adsorber of REE than kaolinite. It is present in sample KS1052.

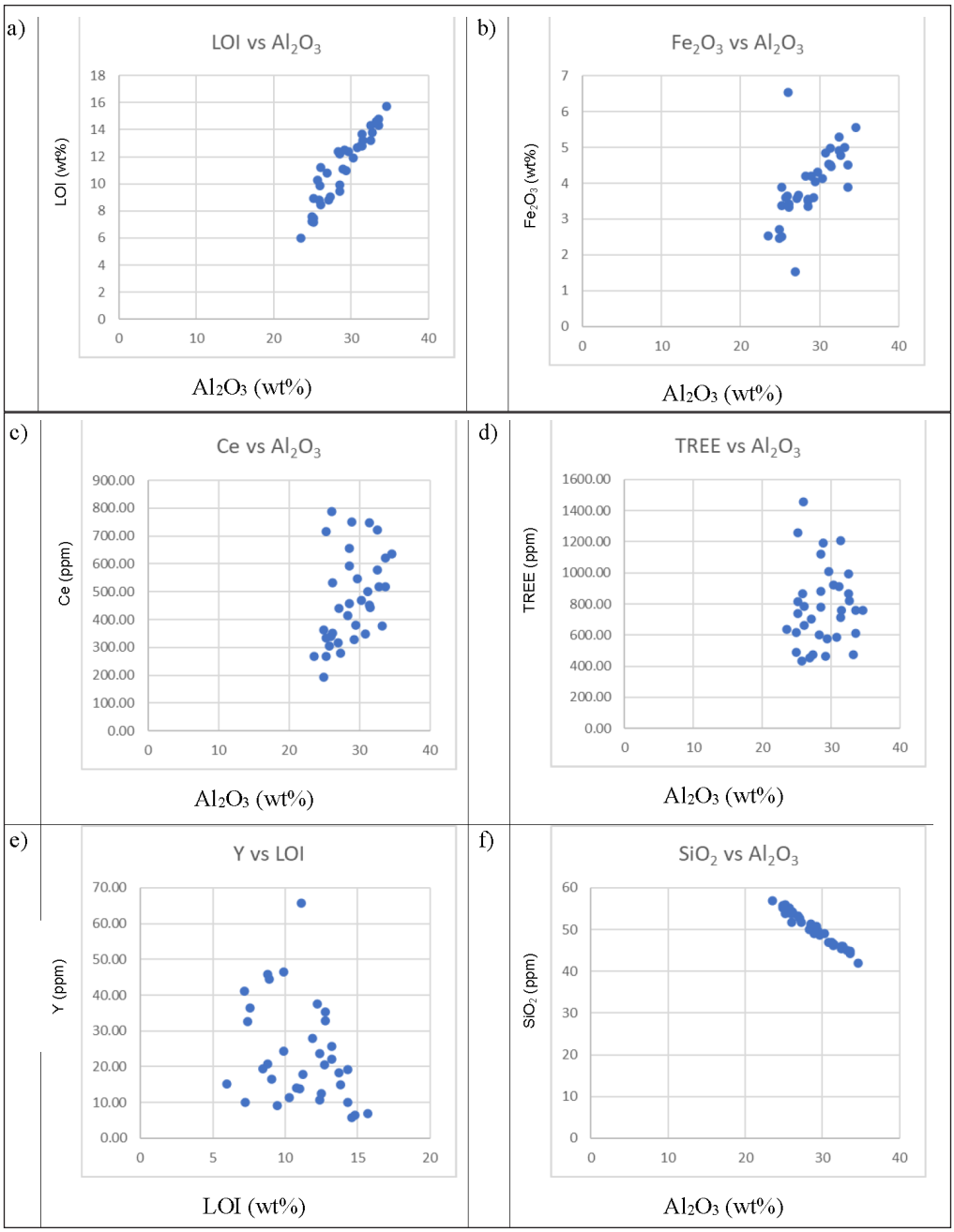

Figure 9: Correlation plots of a) LOI vs Al_2O_3 (coefficient value: 0.94), b) Fe_2O_3 vs Al_2O_3 (0.65), c) Ce vs Al_2O_3 (0.42), d) TREE vs Al_2O_3 (0.04), e) Y vs LOI (-0.32), and f) SiO_2 vs Al_2O_3 (-0.98).

REE contents are higher in the B horizon when compared to the C horizon in most of the soil profiles studied. This corresponds to the higher clay contents in the B horizon. However, C horizon samples KS1060 and KS1081 have higher REE contents than in samples from corresponding upper horizons, which might be due to the formation of REE complexes or secondary REE-bearing phosphate minerals (Murakami & Ishihara, 2008; Sanematsu *et al.*, 2013).

Sanematsu & Watanabe (2016) defines a granitic weathered profile as an ion adsorption-type REE deposit if the profile contains 50% more REE relative to the initial unweathered rock. Since average TREE contents in weathered profiles and in rocks in the study area are 943.85 ppm and 340.89 ppm respectively, the REE deposits in the study area can be considered ion adsorption-type REE deposits.

A study of ion-type REE mineralization in Phuket, Thailand by Sanematsu *et al.* (2013) revealed that REE occurred in minor amounts in Mn and Fe oxides, as well as sulfides and organic matter in weathered profiles. In comparison, the Bukit Enggang area does not show a

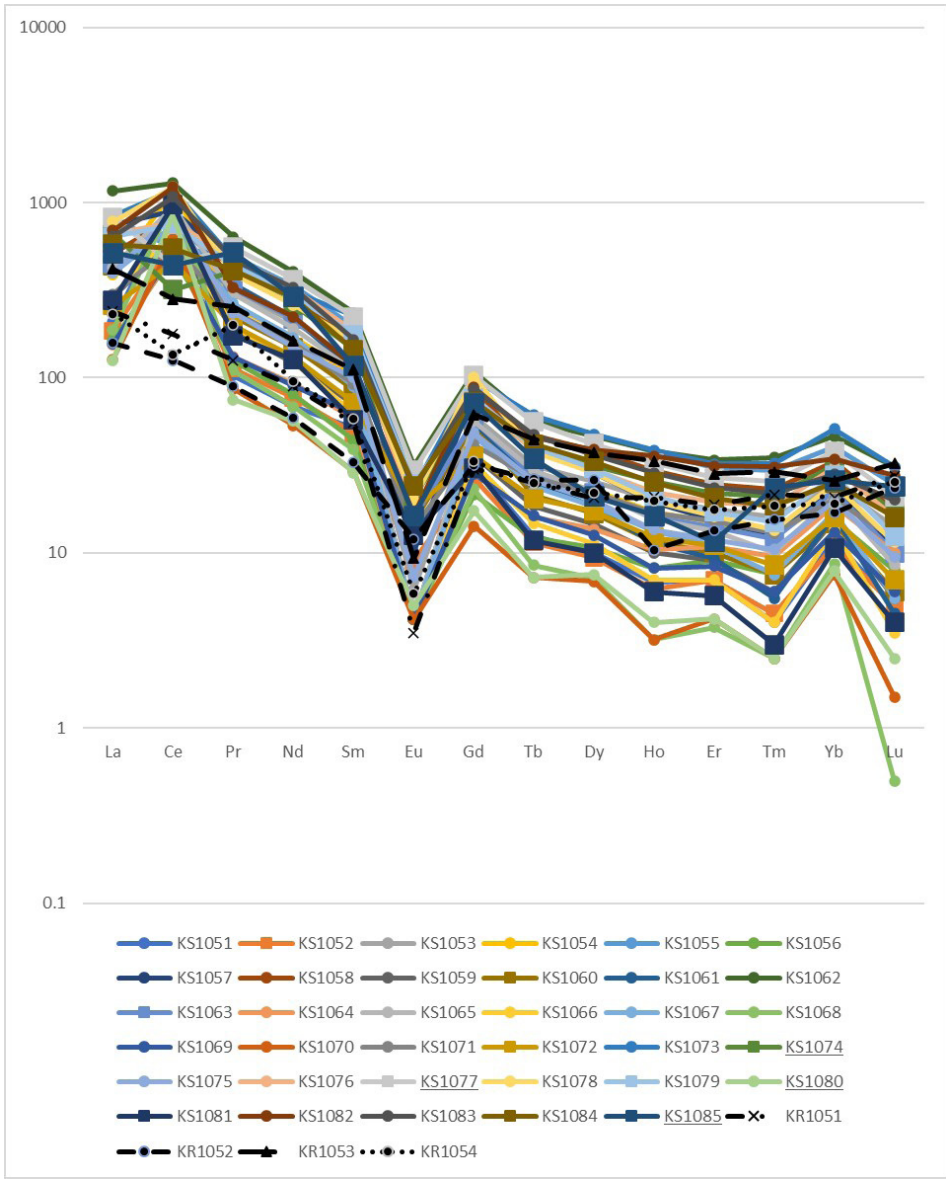

Figure10: Chondrite-normalized diagram of soil (KS1051 to KS1085) and rock samples (KR1051 to KR1054). The lines with square marker denote C horizon soil samples.

significant relationship between Mn and Fe oxides and REE, suggesting that the ion adsorption is the dominant type of mineralization.

Bukit Enggang Granite weathered profiles show greater enrichment in LREE than HREE, as denoted by higher La/Yb in soil samples (12.42 to 47.73) than in the parent rock (13.95 to 24.21). This pattern is similar to that found in central and southern Laos, where there is a depletion in HREE and a slight enrichment in LREE in granitic rocks, this being due to poorly differentiated magma (Sanematsu *et al.*, 2009). Even though the enrichment of LREE during weathering relative to HREE in weathered profiles derived from various parent rocks could be identified (Nesbitt, 1979; Compton *et al.*, 2003), the fractionation of REE is not easily seen in whole-rock geochemical data as it is controlled by the REE-bearing minerals and their resistance to chemical alterations (Sanematsu *et al.*, 2013).

Ce, Eu and La/Yb anomalies

Samples with very high REE contents show positive Ce anomalies. This is likely due to the formation of less soluble Ce^{4+} in oxidizing conditions close to the surface before adsorption onto clay minerals, Fe and Al oxyhydroxides, or the formation of cerianite. The other REEs can only exist as trivalent ions, which remain highly water soluble. This unusual characteristic of Ce also causes its weak association with other REEs, excluding Y. Positive Ce anomalies are also caused by lateritic processes during the weathering of granitic rocks, forming iron oxide minerals such as hematite and goethite (Baioumy & Gilg, 2011; Yusoff *et al.*, 2013).

However, Sanematsu *et al*. (2013) suggested that positive Ce anomaly is an indication of shallow leaching zones of REE, while the higher REE content should occur in accumulation zones in deeper horizons where Ce anomaly should be negative.

Large negative Eu anomalies of rock in this study are indicative of highly differentiated magma. These anomalies are larger than those found in granite in central and southern Laos (Sanematsu *et al.*, 2009). Slightly negative Eu anomalies of all samples, however, suggest the weathering process of granitic profiles occurred in a reducing environment (McLennan, 1989). Baioumy *et al.* (2021) concluded that negative Eu anomalies characterize hydrothermal kaolin in Ipoh, Perak and Gunung Jerai in Kedah. Negative Eu anomalies are also observed in rock samples, hence indicating that the negative anomalies of the Eu in soil samples inherit similar anomalies from parent rock. Aubert *et al.* (2001) and Compton *et al.* (2003) stated that Eu can partition into plagioclase to substitute Sr^{2+}, leading to positive Eu anomalies in feldspar during rock formation. However, removal of feldspar through fractional crystallization during parent magmas fractionation caused the negative Eu anomalies in granites, as studied in Hong Kong (Duzgoren-Aydin & Aydin, 2009).

La/Yb is higher in the soil than in the rock. This indicates that LREE is enriched to a greater degree than HREE by weathering (Sanematsu *et al.*, 2013).

Th and U

Monazite is a phosphate mineral that hosts LREE excluding Eu, and Th and U, with minor amount of Y and HREE (Hinton & Paterson, 1994; Bea *et al.*, 1994; Bea, 1996). Monazite and xenotime are the main controllers of REE evolution in Ca-poor granitic melts. Monazite fractionation favors LREE over HREE, while xenotime fractionation favors HREE (Duc-Tin & Keppler, 2015).

The existence of monazite also results in higher Th content in soil samples, as shown by samples KS1061, KS1064, KS1069 and KS1073. Th content of monazite in Malaysia ranges between 0.25% and 4.08% (Che Zainol Bahri *et al*., 2018) and between 3.12% and 7.48% (Wilbourn, 1925).

The U content in all soil samples is not more than 33.36 ppm. According to the Atomic Energy Licensing Act (1984), if radionuclide of Naturally Occurring Radioactive Materials (NORM) of Th-232 exceeds 1 Bq/g, it is considered as radioactive. 1 Bq/g of Th-232 is equivalent to 246.5 ppm, while U-238 value is equivalent to 91 ppm, assuming the chain is in equilibrium.

CONCLUSION AND RECOMMENDATIONS

The total REE content in weathered profiles in the Bukit Enggang Granite ranges between 432 ppm to 1,455 ppm with an average value of 944 ppm. LREE is more abundant than HREE. The exposed weathered profiles range between 3 to 7 meters thick, containing B and C horizons. The C horizon is thicker than the B horizon, with the presence of relict granite textures and minerals, particularly feldspar. No fresh bedrock is found in the study area, but granite boulders found within the profiles show phaneritic to porphyritic textures consisting of biotite, K-feldspar and quartz as major mineral occurrence, with randomly arranged K-feldspar phenocryst.

Al_2O_3 and LOI in soil range between 23.50 – 34.60% and 5.97 – 15.70% respectively. The most abundant clay mineral in the soil samples is kaolinite, exceeding 49%. REE bearing minerals like monazite, xenotime and zircon are found in most samples but no greater amount than 1.2%.

Both Al_2O_3 and LOI showed strong, positive relationship with Fe_2O_3. The Y element showed positive relationship with REEs except Sc and Ce.

Higher Al_2O_3 and LOI values in soil indicate that the weathering processes involving the conversion of K-feldspar and plagioclase to clay minerals, in particular, kaolinite, occurred under the influence of a reducing environment. This is also indicated by slightly negative Eu anomalies.

The REE content in rock samples are much lower, ranging from 206.70 ppm to 475.07 ppm with an average value of 340.89 ppm. The rock samples have higher SiO_2, Na_2O, K_2O and other oxides compared to Al_2O_3.

Based on the above findings, the REE deposits in the study area can be regarded as ion adsorption-type deposits. The enrichment of REE in weathered profiles is due to the dissolution of soluble REE-bearing minerals such as fluorapatites and fluorocarbonates in the upper, oxidized parts of the profiles, and adsorption of dissolved REEs onto clays in the lower parts.

There may be zones of REE accumulation that were deeper than the 5 meter sampling depth, since all soil samples show positive Ce anomalies. Future studies should include deeper sampling, and the use of geophysical methods to determine the actual depth to the unaltered bedrock.

ACKNOWLEDGEMENTS

We acknowledge The Director General and The Deputy Director General of The Department of Mineral and Geoscience Malaysia (JMG) for giving the permission for this study to be published. We are also grateful to Dr. Sia Say Gee, Mr. Mohd Zahar Ibrahim and JMG REE Core Group members for helpful advice, and the anonymous reviewers for constructive comments and suggestions which helped us to improve the article.

AUTHORS CONTRIBUTION

EJ performed field mapping and sampling. MSF and MFZ performed XRD analysis and interpretations. FAF conducted geochemical result interpretation and wrote the whole manuscript. HA, AS, AHAR and AA contributed to critically reviewing the manuscript and contributing ideas to improve the paper.

CONFLICT OF INTEREST

The authors declare there is no conflict of interest.

REFERENCES

Abdul Rahman, A.H., 2011. Tepoh Clay, Terengganu: descriptions and effects on brick calcination process (in Malay). MSc Thesis, UKM, Malaysia (unpublished thesis).

Abdul Rahman, A.H., Sibon, M. & Ariffin, H., 2020. Reconnaissance study on rare earth elements in northern Kedah, Kedah and Perlis (in Malay). Department of Mineral and Geoscience Malaysia, Putrajaya, Malaysia (unpublished report).

Abdul Rahman, A.H., Sibon, M. & Hasan, M.S., 2018. Reconnaissance study on rare earth elements in southern Kedah (in Malay). Department of Mineral and Geoscience Malaysia, Putrajaya, Malaysia (unpublished report).

Abdul Rahman, A.H., Sibon, M., & Hasan, M.S., 2019. Reconnaissance study on rare earth elements in northern Perak, Perak and parts of eastern Kedah, Kedah (in Malay). Department of Mineral and Geoscience Malaysia, Putrajaya, Malaysia (unpublished report).

Alonso, E., Sherman, A.M., Wallington, T. J., Everson, M.P., Field, F.R., Roth, R. & Kirchain, R.E., 2012. Evaluating rare earth element availability: A case with revolutionary demand from clean technologies. Environmental Science and Technology, 46, 3406-3414.

ASM, 2014. Blueprint for the establishment of rare earth-based industries in Malaysia: summary for policy maker. Akademi Sains Malaysia, Kuala Lumpur, Malaysia.

Atomic Energy Licencing Act, 1984. Federal Constitution of Malaysia.

Aubert, D., Stille, P. & Probst, A., 2000. REE fractionation during granite weathering and removal by waters and suspended loads: Sr and Nd isotopic evidence. Geochemica et Cosmochimica Acta, 65, 387-406.

Baioumy, H. & Gilg, A., 2011. Pisolitic flint kaolin from Kalabsha, Egypt: a laterite derived facies. Sed. Geol., 236, 141-152.

Baioumy, H. Farahat, M., Arifin, M.H., Anuar, M.N.A. & Al-Kahtany, K., 2021. Hypogene kaolin deposits from felsic intrusive rocks (Peninsular Malaysia) with special reference to rare earth elements and stable isotopes geochemistry. Geosciences Journal, https://doi.org/10.1007/s12303-021-0003-9.

Bao, Z. & Zhao, Z., 2008. Geochemistry of mineralization with exchangeable REY in the weathering crusts of granitic rocks in South China. Ore Geology Reviews, 33, 519-535.

Bea, F., 1996. Residence of REE, Y, Th and U in granites and crustal protoliths; Implications for the chemistry of crustal melts. Journal of Petrology, 37, 521-552.

Bea, F., Pereira, M.D., Corretge, L.G. & Fershtater, G.B., 1994. Differentiation of strongly peraluminous, perphosphorous granites: The Pedrobernardo pluton, central Spain. Geochimica et Cosmochimica Acta, 58, 2609-2627.

Bradford, E.F., 1972. The geology and mineral resources of the Gunung Jerai area, Kedah. District Memoir 13. Geological Survey of Malaysia. Kuala Lumpur, Malaysia. 156 p.

Chappell, B.W. & White, A.J.R., 2001. Two contrasting granite types; 25 years later. Australian Journal of Earth Sciences, 48, 489-499.

Che Zainol Bahri, C.N.A., Ismail, A.F., Ab Majid, A., Mohd Ruf, M.I.F. & Al-Areqi, W.M., 2018. Extraction and purification of thorium oxide from monazite mineral. Sains Malaysiana, 47, 1873-1882.

Compton, J.S., White, R.A. & Smith, M., 2003. Rare earth element behavior in soils and salt pan sediments of a semi-arid granitic terrain in the Western Cape, South Africa. Chem. Geol., 201, 239-255.

Connelly, N.G. & Damhus, T., 2005. Nomenclature of inorganic chemistry: IUPAC recommendations. RSC Publishing, London, England. 51 p.

Duc-Tin, Q. & Keppler, H., 2015. Monazite and xenotime solubility in granitic melts and the origin of the lanthanide tetrad effect. Contributions to Mineralogy and Petrology, 169, 26 p.

Duzgoren-Aydin, N.S. & Aydin, A., 2009. Distribution of rare earth elements and oxyhydroxide phases within a weathered felsic igneous profile in Hong Kong. Journal of Asian Earth Sciences, 34, 1-9.

Fauzi, F.A., 2018. Reconnaissance study on rare earth elements in Kedah (Phase 1). Department of Mineral and Geoscience Malaysia, Putrajaya, Malaysia (unpublished report).

Flinter, B.H., Butler, J.R. & Harral, G.M., 1963. A study of alluvial monazite from Malaya. The American Mineralogist, 48, 1210-1226.

Hatch, G.P., 2012. Dynamics in the global market for rare earths. Elements, 8, 341-346.

Hinton, R.W. & Paterson, B.A., 1994. Crystallisation history of granitic magma: Evidence from trace element zoning. Mineralogical Magazine, 58, 416-417.

Hosking, K.F.G., 1973. The primary tin mineralization patterns of West Malaysia. Bulletin of the Geological Society of Malaysia, 6, 297-308.

Husin, Z., Ab. Ghani, M.Z., Abdul Rahman, A.H., Eki, A., Ariffin, H, Kassim, M., Ibrahim, I., Ibrahim, K. & Jinap, J.J., 2015. Guidelines rare earth element explorations (in Malay). Department of Mineral and Geoscience Malaysia. 80 p.

Ishihara, S., Sawata, H., Arpornsuwan, S., Busaracome, P. & Bungbrakearti, P., 1979. The magnetite-series and ilmenite-series granitoids and their Bearing on tin mineralization, particularly of the Malay Peninsula region. Bulletin of the Geological Society of Malaysia, 11, 103-110.

Ishihara, S., Renmin, H., Hoshino, M. & Murakami, H., 2008. REE abundance and REE minerals in granitic rocks in the Nanling Range, Jiangxi Province, Southern China, and generation of the REE-rich weathered crust deposits. Resource Geol., 58, 355-372.

JMG, 2014. Geological map of Kedah. Kuala Lumpur, Malaysia, Department of Mineral and Geoscience, Malaysia.

KeTSA, 2021. Kerangka Pelan Transformasi Industri Mineral Negara 2021-2030. Kementerian Tenaga Dan Sumber Asli Malaysia, Putrajaya. 5 p.

Liu, L., Hu, R., Zhong, H., Yang, J., Kang, L., Zhang, X., Fu, Y., Mao, W. & Tang, Y., 2020. Petrogenesis of multistage S-type granite from the Malay Peninsula in the Southeast Asian Tin Belt and their relationship to Tethyan evolution. Gondwana Research, 84, 20-37.

McLennan, S. M., 1989. Rare earth elements in sedimentary rocks: Influence of provenance and sedimentary processes. Reviews in Mineralogy and Geochemistry, 21(1), 169-200.

Mohd Hassan, M.Z.., 1989. Report on follow-up exploration on geochemical-radiometric anomalies in Peninsular Malaysia (in Malay). Regional Mineral Exploration Project Report 13-18/1988 and 1-6/1989, Ministry of Primary Industries (unpublished report).

Murakami, H. & Ishihara, S., 2008. REE mineralization of weathered crust and clay sediment on granitic rocks in the Sanyo belt, SW Japan and southern Jiangxi province, China. Resource Geol., 58, 373-401.

Neary, C.R. & Highley, D.E., 1984. The economic importance of the rare earth elements. In: Henderson, P. (Ed.), Rare earth element geochemistry. Elsevier, Amsterdam, Netherlands. 423–466.

Nesbitt, H.W., 1979. Mobility and fractionation of rare earth elements during weathering of a granodiorite. Nature, 279, 206-210.

Ng, S.W.P., Chung, S.L., Robb, L.J., Searle, M.P., Azman A. Ghani, Whitehouse, M.J., Oliver, G.J.H., Sone, M., Gardiner, N.J. & Muhammad H. Roslee, 2015. Petrogenesis of Malaysian granitoids in the Southeast Asian Tin Belt: Part 1. Geochemical and Sr-Nd isotopic characteristics. Geological Society of America Bulletin, 127, 1209-1237.

Robb, L.J., 2019. The Geology of Tin Deposits with Special Reference to Tin Mineralisation in Peninsular Malaysia. National Tin Conference 2019, 1 p.

Sanematsu, K., Murakami, H., Watanabe, Y., Duangsurigna, S. & Vilayhack, S., 2009. Enrichment of rare earth elements (REE) in granitic rocks and their weathered crusts in central and southern Laos. Bulletin of the Geological Survey of Japan, 60, 527-558.

Sanematsu, K., Kon, Y., Imai, A., Watanabe, K. & Watanabe, Y., 2013. Geochemical and mineralogical characteristics of ion-adsorption type REE mineralization in Phuket, Thailand. Miner. Deposita, 48, 437-451.

Sanematsu, K. & Watanabe, Y., 2016. Characteristics and genesis of ion adsorption-type rare earth element deposits. In: Verplank, P.L. & Hitzman, M.W. (Eds.), Review In Economic Geology: Rare Earth and Critical Elements In Ore Deposits, 18. https://doi.org/10.5382/Rev.18.03.

Sengupta, D. & Van Gosen, B.S., 2016. Chapter 4: Placer-type rare earth element deposits. In: Verplanck, P.L., & Hitzman, M.W. (Eds.), Rare earth and critical elements in ore deposits. Reviews in Economic Geology. Virginia, USA. 365 p.

Sun, S.S. & McDonough, W.F., 1989. Chemical and isotopic systematics of Oceanic Basalts: Implications for mantle composition and processes. In: Saunders, A.D. & Norry, M.J. (Eds.), Magmatism in the Ocean Basins. Geological Society London Special Publications, 42, 313-345.

Tampubolon, A., Syafri, I, Rosana, M.F., & Yuningsih, E.T., 2022. The occurrence of primary REE minerals and their paragenesis within S-type granite and quartz vein, South Bangka, Bangka Belitung Islands, Indonesia. Journal of Electrical Electronics Engineering, 1, 64-86.

Teoh, L.H., 1992. Geology and mineral resources of Sungai Tiang area, Kedah Darul Aman. Geological Survey Malaysia Map Report 5. Geological Survey of Malaysia.

Wan Hassan, W.F., 1989. Some characteristics of the heavy detrital minerals from Peninsular Malaysia. Bulletin of the Geological Society of Malaysia, 24, 1-12.

Willbourn, E.S., 1925. A list of minerals found in British Malaya together with a description of their properties, composition, occurrences and uses. Journal of the Malayan Branch of the Royal Asiatic Society, 3, 57-100.

Wu, C., Huang, D. & Guo, Z., 1990. REE geochemistry in the weathered crust of granites, Longnan area, Jiangxi province. Acta Geol. Sinica, 3, 193–210.

Yang, J., Zhou, M., Zhong, H., Williams-Jones, A.E., Liu, L., Zhang, X., Fu, Y. & Mao, W., 2020. Granite-related tin metallogenic events and key controlling factors in Peninsular Malaysia, Southeast Asia: New insights from Cassiterite U-Pb dating and zircon geochemistry. Economic Geology, 115, 581-601.

Yusoff, Z.M., Ngwenya, B. & Parsons, I., 2013. Mobility and fractionation of REEs during deep weathering of geochemically contrasting granites in a tropical setting, Malaysia. Chemical Geology, 349-350, 71-86.

Zhou, B., Li, Z. & Chen, C., 2017. Global potential of rare earth resources and rare earth demand from clean technologies. Minerals, 2017, 203–217.

Manuscript received 10 November 2022;
Received in revised form 18 May 2023;
Accepted 24 May 2023
Available online 29 November 2023